Received: 17 September 2021 | Revised: 12 January 2022 | Accepted: 22 February 2022

DOI: 10.1002/jnr.25042

RESEARCH ARTICLE

JOURNAL OF Neuroscience Research

Calcium signaling in individual APP/PS1 mouse dentate gyrus astrocytes increases *ex vivo* with Aβ pathology and age without affecting astrocyte network activity

Christiaan F. M. Huffels[1] | Lana M. Osborn[2] | Natalie L. M. Cappaert[2] | Elly M. Hol[1]

[1]Department of Translational Neuroscience, University Medical Center Utrecht Brain Center, Utrecht University, Utrecht, The Netherlands

[2]Swammerdam Institute for Life Sciences, Center for Neuroscience, Cellular and Computational Neuroscience, University of Amsterdam, Amsterdam, The Netherlands

Correspondence
Elly M. Hol, Department of Translational Neuroscience, University Medical Center Utrecht Brain Center, Utrecht University, Utrecht, The Netherlands.
Email: e.m.hol-2@umcutrecht.nl

Funding information
This work was supported by ZonMW [733050816]: The Netherlands Organization for Health Research and Development, Dementia Research and Innovation Program "Memorabel"

Abstract

Astrocytes are critical for healthy brain function. In Alzheimer's disease, astrocytes become reactive, which affects their signaling properties. Here, we measured spontaneous calcium transients *ex vivo* in hippocampal astrocytes in brain slices containing the dentate gyrus of 6- (6M) and 9-month-old (9M) APPswe/PSEN1dE9 (APP/PS1) mice. We investigated the frequency and duration of calcium transients in relation to aging, amyloid-β (Aβ) pathology, and the proximity of the astrocyte to Aβ plaques. The 6M APP/PS1 astrocytes showed no change in spontaneous calcium-transient properties compared to wild-type (WT) astrocytes. 9M APP/PS1 astrocytes, however, showed more hyperactivity compared to WT, characterized by increased spontaneous calcium transients that were longer in duration. Our data also revealed an effect of aging, as 9M astrocytes overall showed an increase in calcium activity compared to 6M astrocytes. Subsequent calcium-wave analysis showed an increase in sequential calcium transients (i.e., calcium waves) in 9M astrocytes, suggesting increased network activity *ex vivo*. Further analysis using null models revealed that this network effect is caused by chance, due to the increased number of spontaneous transients. Our findings show that alterations in calcium signaling in individual hippocampal astrocytes of APP/PS1 mice are subject to both aging and Aβ pathology but these do not lead to a change in astrocyte network activity. These alterations in calcium dynamics of astrocytes may help to understand changes in neuronal physiology leading to cognitive decline and ultimately dementia.

KEYWORDS
aging, Alzheimer's disease, APP/PS1, astrocytes, calcium imaging, calcium waves, null models, RRID:MMRRC_016992-MU, RRID:SCR_001622, RRID:SCR_002798, RRID:SCR_013726

Christiaan F. M. Huffels and Lana M. Osborn contributed equally to this work.
Edited by Junie Paula Warrington and Stephen J. Crocker. Reviewed by Cory M. Willis and Christoph Proschel

1 | INTRODUCTION

Alzheimer's disease (AD) is the most prevalent form of dementia and is characterized by prominent glial and neuropathological changes (Braak & Braak, 1991, 1996). Amyloid-β (Aβ) oligomers are thought to be the early initiators that may trigger these changes, including astrocyte reactivity (DaRocha-Souto et al., 2011; Hsia et al., 1999; Lambert et al., 1998). Classically, morphological changes in astrocytes and an increased expression of the intermediate filament protein glial fibrillary acidic protein (GFAP) characterize astrocyte reactivity (Diedrich et al., 1987; Eng et al., 1971; Prince et al., 1993; Shafit-Zagardo et al., 1988; reviewed by Escartin et al., 2021). As astrocytes are part of the tripartite synapse, they are closely involved in regulating neuronal physiology by controlling many processes, including neurotransmitter recycling, energy metabolism, and maintaining K^+ homeostasis (reviewed by Verkhratsky & Nedergaard, 2018). Astrocyte reactivity has been implicated to have both beneficial and adverse effects (Kobayashi et al., 2018). Adverse effects become particularly apparent upon prolonged astrocyte reactivity and result in altered astrocyte properties leading to neuronal hyperactivity and reduced neuronal support, ultimately causing aberrant cognitive functions, and thereby aggravating AD pathogenesis (reviewed by Hol & Pekny, 2015; Osborn et al., 2016; Pekny et al., 2016). Although advances have been made in clarifying the role of reactive astrocytes in causing these pathological events, the exact underlying mechanisms remain complex and need to be further investigated (reviewed by Escartin et al., 2021).

To regulate neuronal activity, astrocytes communicate through calcium transients, forming wave-like patterns within the astrocyte syncytium (Cornell-Bell et al., 1990; Kang et al., 1998; Porter & McCarthy, 1996). A few reports have shown that calcium signaling in astrocytes appears to be dysregulated as a consequence of astrocyte reactivity. For instance, cortical astrocytes in APPswe/PSEN1dE9 mice show elevated calcium levels, independent of plaque proximity, and exhibit more frequent calcium transients that are synchronized in waves across longer distances (Kuchibhotla et al., 2009). These calcium transients continue throughout the astrocyte network and appear to be directly affected by neuronal activity and purinergic signaling (Delekate et al., 2014; Kuchibhotla et al., 2009). Although aberrant astrocyte calcium signaling is known to affect neuronal activity, the exact physiological implications of aberrant astrocyte calcium signaling are diverse and complex and remain to be fully discovered (Delekate et al., 2014; Shigetomi et al., 2016; reviewed by Verkhratsky, 2019).

The transentorhinal and entorhinal cortices (ECs) are among the first brain regions to be severely affected by AD pathology (Braak et al., 1996; Braak & Braak, 1991, 1996). Astrocytes in these cortices appear reactive in all patients showing AD pathology, irrespective of whether clinical symptoms were present or not (Kobayashi et al., 2018). Afferents from the ECs project onto the hippocampal dentate gyrus (DG), an area essential for spatiotemporal encoding and long-term memory formation (Madroñal et al., 2016). Studies show that the presence of reactive astrocytes in the ECs not only coincides with the appearance of Aβ plaques in the ECs, but also in the DG (Kamphuis et al., 2014; Olabarria et al., 2010). As such, neurodegeneration in the ECs is associated with reduced synapse and neuron density in the DG (Bertoni-Freddari et al., 2003; Masliah et al., 1994; reviewed by Masliah et al., 2006). Furthermore, various studies have indicated that reactive astrocytes are present throughout various stages of AD progression in the DG (Olabarria et al., 2010). However, whether the calcium-signaling properties of astrocytes in the DG are changed in AD is still unknown.

Significance

Alzheimer's disease (AD) is the most prevalent form of dementia and is characterized by astrocyte reactivity. Aberrant astrocyte calcium signaling affects neuronal support in various brain regions. However, whether calcium signaling properties of astrocytes in the dentate gyrus (DG) are changed in AD is still unclear. This study revealed that calcium signaling in individual APP/PS1 DG astrocytes increases with age and amyloid-β (Aβ) pathology *ex vivo*. However, this increase did not affect astrocyte network activity. Together, the data in this study aid the understanding of astrocyte pathophysiology in the DG following the early and prolonged exposure to Aβ pathology.

In this study, we aimed at understanding how calcium activity in reactive astrocytes in the DG changes in response to Aβ pathology. For this, we used the established APPswe/PSEN1dE9 AD mouse model (reviewed by Smit et al., 2021) expressing a GCaMP3 calcium indicator downstream of the GFAP promoter. This model is characterized by the gradual development of Aβ-plaque pathology (Jankowsky et al., 2004). The first Aβ plaques in the DG are detectable at 5 months, corresponding to early-stage AD, after which plaque deposition increases over time and resembles mid-stage AD by 9 months (Jankowsky et al., 2004; Kamphuis et al., 2012). Using this model, we assessed *ex-vivo* astrocyte calcium activity in the DG of both 6- and 9-month-old (6M, 9M) APPswe/PSEN1dE9 mice and WT littermates, allowing us to follow changes during AD progression and gliosis. We characterized the properties of single calcium events in all groups to determine whether astrocyte calcium activity is affected by Aβ pathology or aging. At the same time, we assessed whether Aβ-plaque proximity was involved in the dysregulation of astrocyte calcium signaling. Furthermore, we performed extensive calcium-wave analysis to determine whether reactive astrocytes in the DG show alterations in calcium-wave patterns similar to what has been observed in the cortex.

2 | MATERIALS AND METHODS

2.1 | Animals

Hemizygous double-transgenic APPswe/PSEN1dE9 (APP/PS1) mice (strain B6.Cg-Tg[APPswe, PSEN1dE9]85Dbo/Mmjax; stock number 034832-JAX; https://jaxmice.jax.org) (Jankowsky et al., 2004); originally

received from Dr. Borchelt and back-crossed to C57BL/6) were crossed with homozygous GCaMP3f/f mice (https://www.jax.org/strain/014538). Mice from these litters were back crossed to homozygous GCaMP3f/f mice to maintain a hemizygous APP/PS1 line with homozygous GCaMP3f/f mice. APP/PS1$^{-/+}$GCaMP3$^{+/+}$ mice were then crossed with GFAP-CreERT2$^{+/+}$ mice (RRID:MMRRC_016992-MU, https://www.mmrrc.org/catalog/sds.php?mmrrc_id=16992). 6M and 9M male and female APP/PS1$^{-/+}$GCaMP3$^{+/+}$GFAP-CreERT2$^{-/+}$ were then used for experiments and compared against APP/PS1$^{-/-}$GCaMP3$^{+/+}$GFAP-CreERT2$^{-/+}$ control littermates of similar age. The genotype was determined by performing real-time polymerase chain reaction. Animals were then assigned to the experimental or control group in a 1:1 male–female ratio. Throughout the rest of the experiment, researchers were blinded for genotype and age. Intraperitoneal injection of 120 mg/kg of Tamoxifen (Tocris, cat. no. 0999) dissolved in corn oil (20 mg/ml) was administered for 4 consecutive days, starting 2 weeks before recording. All animals were handled regularly and were group housed (max. 6) under standard laboratory conditions (12-hr light/dark cycle, 21°C, 50% humidity) in the presence of cage enrichment (nesting material). Food and water were provided *ad libitum*. All experiments were performed following protocols and guidelines approved by the Institutional Animal Care and Use Committee (UvA-DEC/IvD Utrecht) operating under standards set by EU Directive 2010/63/EU.

2.2 | Slice preparation

Acute horizontal slices of the hippocampus were obtained from 6M and 9M APP/PS1$^{-/+}$ × GCaMP3$^{+/+}$ × GFAP-CreERT2$^{-/+}$ (APP6 and APP9) mice and littermate controls (APP/PS1$^{-/-}$ × GCaMP3$^{+/+}$ × GFAP-CreERT2$^{-/+}$; WT6 and WT9). Following decapitation, the brain was rapidly removed and stored in ice-cold oxygenated modified artificial cerebrospinal fluid (mACSF in mM: 87 NaCl, 60 sucrose, 2.5 KCl, 1.25 NaH_2PO_4, 7 $MgCl_2$, 0.5 $CaCl_2$, 10 D-glucose, 25 $NaHCO_3$, pH 7.4). Thick slices of 290 μm were cut with a vibratome (VT1000S, Leica) and transferred to mACSF of 35°C to recover for 20 min. Sulforhodamine 101 (SR101, S7635, Sigma) was added to a concentration of 1 μM and the slices were incubated to selectively stain astrocytes at room temperature (RT) for 20 min (Kafitz et al., 2008; Nimmerjahn et al., 2004). Next, slices were transferred to ACSF (in mM: 126 NaCl, 3 KCl, 2 $CaCl_2$, 2 $MgSO_4$, 1.25 NaH_2PO_4, 10 D-glucose, and 26 Na_2HCO_3) and kept at RT. During recording, slices were continuously perfused with ACSF (2.5 ml/min) at a temperature of 28°C. All solutions mentioned were continuously oxygenated with 95% O_2–5% CO_2.

2.3 | Calcium imaging

Cells were visualized with an upright microscope (SliceScope Pro 6000, Scientifica, UK), equipped with oblique illumination and a 40× water immersion objective. Images were acquired with an Orca-Flash 4.0 v2 digital CMOS camera (Hamamatsu Photonics, Japan) and Hokawo imaging acquisition software (Hamamatsu Photonics, Japan) running in external trigger mode. Images were acquired over 210 s with a sample frequency of 8 Hz and 2 × 2 binned (1,048 × 1,048 pixels). Astrocytes were visually identified by their GCaMP3 positivity, expressed under the GFAP promoter, using a 470 nm LED and 525 nm emission filters. To ensure GCaMP3$^+$ cells were astrocytes, we additionally checked for SR101 positivity using a 585 nm LED (pE-100, CoolLED, UK) and mCherry-Texas Red filter cubes (Chroma, USA). Likewise, Aβ plaques were visually identified by their rugged, dense appearance with a clear-defined border. The fluorescent marker methoxy-X04 normally used for identifying plaques (Klunk et al., 2002) in live brain tissue could not be used during experiments, as this would interfere with the wavelength of the GCaMP3 signals. However, control experiments were performed by staining brain slices with methoxy-X04 (10 μM, in 0.01% DMSO, cat. #4920, Tocris) to make sure tissue with a rugged, dense appearance were indeed Aβ plaques.

2.4 | Calcium-data analysis

The fluorescence signal was quantified by manually selecting GCaMP3$^+$ somatic regions of interest (ROIs) from the mean image made from all frames. Selected ROIs were then checked for SR101 positivity and only GCaMP3$^+$/SR101$^+$ cells were used in subsequent analyses. The average GCaMP3 signal from all pixels within the ROI was determined for all frames and used as the raw signal for further analysis utilizing in-house MATLAB scripts running in version 2014b (RRID:SCR_001622). Raw signals were fitted with an eighth-order polynomial which was then subtracted from the raw signal (ΔF) and subsequently divided by the fit (F) to give the change in fluorescence over time ($\Delta F/F$) as adapted from Balkenius et al. (2015). Subsequently, the value in baseline was determined for each astrocyte individually, by taking the average signal per eight consecutive frames and binning these values to determine a distribution of baseline values. If this resulted in a right-skewed intensity distribution, that is the bin with the greatest number of values fell within the lower third of the intensity distribution, the average of all values in this lower third was set as the baseline. Bins above this lower third contained the calcium-transient peaks. Alternatively, the distribution was observed to be Gaussian and representative of background noise, in which case the average of the entire signal was used to set the baseline value. To determine the frequency and timing of calcium transients, peaks were detected using the built-in MATLAB function *findpeaks*. Transients included for analysis had to meet three criteria: (1) the height of the peak had to be at least 2.5 times the standard deviation of the baseline signal ("*MinPeakHeight*"); (2) the minimal time between two peaks had to be at least 3 s ("*MinPeakDistance*"); and (3) the peaks need to have a minimum relative importance of 1 standard deviation of the baseline ("*MinPeakProminence*"). Next, it was determined whether the transients detected were single events or whether the transient contained multiple peaks before returning to baseline. Multiple peaks within one transient were defined

as supra-events and the width at half-height of each transient was used to estimate the duration of these supra-events. Single-event durations were determined by finding the points at which the signal crossed 2.5 times the standard deviation of the baseline in either direction. The analyses of acquired data were carried out using custom-made MATLAB scripts running in version 2019b (RRID:SCR_001622).

2.5 | Calcium-wave analysis

Next, astrocyte waves were identified. First, two astrocytes were identified as pairs if they were no more than 50 μm apart and showed successive transients between 0.5 and 3 s (Delekate et al., 2014; Oberheim et al., 2009). This pairwise step was then further carried out to determine how far the sequence of paired transients reached, up to and including eight astrocytes, with each subsequent pair meeting the above criteria. Events matching these criteria and involving three or more astrocytes were considered waves. If a sequence of astrocytes was present in a longer wave (e.g., in case a four-astrocyte sequence contained the same astrocytes in the same order as a five-astrocyte sequence), then this sequence was eliminated from the shorter wave to eliminate redundancy and determine unique wave combinations. The average number of cell pairs was determined by calculating how often a single astrocyte received input from and sent output to another astrocyte, following the same above criteria. The recurrence of certain astrocyte pairs was determined, and unique seeds were identified by establishing which astrocytes routinely initiated the formation of wave combinations. Wave analysis was done using custom-made MATLAB scripts running in version 2019b (RRID:SCR_001622).

2.6 | Null models

Pseudo-randomized null models were created by generating permutations on the same data used for calcium-wave analysis, as previously described in Farine (2017). Each permutation contained the same number of astrocytes and calcium events as present in the raw data but differed in the timestamps at which the events occurred. In total, 1,000 pseudo-randomized null models were generated per brain slice. Subsequently, calcium-wave analysis as described above was performed on every null model. The average null-model group distribution of relevant astrocyte network parameters was then compared to the matching value in the observed data. The observed value was considered significantly different when it fell within the outermost 5% of the obtained distribution, in which case we concluded that the observed pattern was significantly different from chance level. Null models were generated using custom-made MATLAB scripts running in version 2019b (RRID:SCR_001622).

2.7 | Statistics

Reported numerical values are given as mean and standard error of the mean (±*SEM*), unless mentioned otherwise. As analysis revealed no sex differences (data not shown), male and female data were combined. The sample size was estimated by performing a power analysis with G*Power 3.1 (RRID:SCR_013726) using values found in literature. Statistical analyses were performed in GraphPad Prism 6 (RRID:SCR_002798). First, outliers were identified using the built-in GraphPad Prism outlier identifier (ROUT, $Q = 1\%$). This resulted in the exclusion of a single APP9 brain slice for calcium-wave analysis. No animals were excluded from analyses. Statistical analyses between two groups were made using an unpaired Student's *t* test. Statistical comparisons between three or more groups were made using a one-way analysis of variance (ANOVA). When comparison involved two factors and two or more groups, a two-way ANOVA was used. Whenever a *F*-test or Bartlett's test for equal variances obtained $p < 0.05$, nonparametric equivalents were used. The Mann–Whitney and Kruskal–Wallis tests were used as nonparametric equivalents for the unpaired Student's *t* test and one-way ANOVA, respectively. For each comparison, the statistical test used is indicated in the results section. Post-hoc multiple comparison tests to determine group differences were used where appropriate and are indicated when relevant. For all statistical evaluations, we assumed that $p < 0.05$ indicates rejection of the null hypothesis. The number of transients (n_t), cells (n_c), slices (n_s), and animals (N) used for analyses are mentioned in text at the relevant comparison and are additionally listed in the figure legends.

3 | RESULTS

3.1 | Astrocyte calcium transients

To determine differences in calcium transients between astrocytes in APP/PS1 mice and WT littermates, we recorded fluorescence signals from GCaMP3$^+$/SR101$^+$ astrocytes in the DG of hippocampal slices. By labeling astrocytes with the astrocyte-specific dye SR101, we ensured that the analyzed fluorescence signals were originating from astrocytes, as the GFAP promoter driving GCaMP3 can be leaky (reviewed by Brenner & Messing, 2021). Before recording, Aβ plaques were identified in brain slices by their rugged, dense appearance with a clear-defined border using oblique illumination (Figure 1a). Control experiments indicate that these structures are indeed Aβ plaques, as they co-localize with fluorescence signals (Figure S1) obtained after slice treatment with 10 μM methoxy-X04, which is normally used to stain Aβ plaques in live brain tissue (Klunk et al., 2002). Identifying Aβ plaques in brain slices allowed us to make the distinction between calcium activity recorded from astrocytes near Aβ plaques (≤ 80 μm) and those further away. The image plane used for recording the somatic calcium transients was set at the

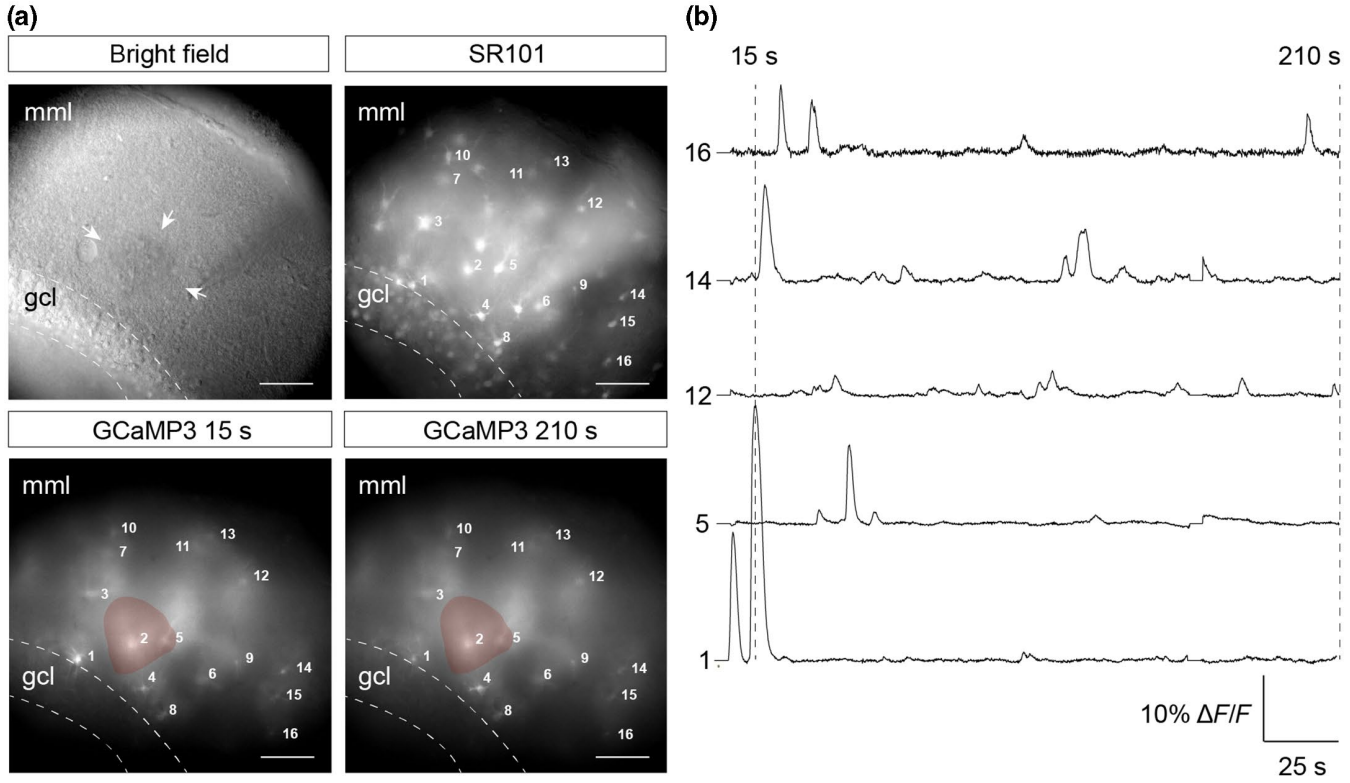

FIGURE 1 Genetically encoded GCaMP3$^+$ reveals detectable somatic changes in calcium over time *ex vivo*. (a) Plaques in APP/PS1 mice (APP9 depicted) were identified using oblique illumination characterized by a rugged, dense appearance with a defined border (upper left panel, white arrows; lower left and right panel, red area). Astrocytes were identified as SR101$^+$ (upper right panel, numbered cells GCaMP3$^+$). Not all SR101$^+$ cells are GCaMP3$^+$. Recorded astrocytes showed clear fluctuations in somatic calcium as can be seen in cell 1 at 15 s (lower left panel) vs. 210 s (lower right panel), scalebar 50 μm. (b) Transient changes in somatic calcium ($\Delta F/F$) were recorded as changes in fluorescence over time; cell numbers correspond with those in a. gcl, granule cell layer; mml, middle molecular layer

focal plane with the greatest number of GCaMP3$^+$/SR101$^+$ astrocytes in focus. Not all SR101$^+$ cells were GCaMP3$^+$, as can be seen by comparing the SR101$^+$ staining and GCaMP3 signal (Figure 1a, right upper panel vs. lower panels). Astrocytes showed clear changes in somatic calcium levels over time, as can be observed by comparing the lower left (15 s) and lower right (210 s) panel of Figure 1a. For instance, a change in calcium intensity from high to low can be observed in astrocyte number one. For a select group of astrocytes annotated in Figure 1a, the corresponding calcium trace is shown in Figure 1b, including the 15 and 210 s timestamps. These data show that measurable somatic changes in calcium intensity over time could be recorded from GCaMP3$^+$/SR101$^+$ astrocytes.

3.2 | The frequency and duration of calcium transients in *ex-vivo* astrocytes increases with age and Aβ pathology

To assess whether DG astrocytes have a different physiological phenotype during the early- and mid-stages of AD progression, we quantified the relative frequency and duration of somatic calcium transients in WT6, APP6, WT9, and APP9 hippocampal slices. Visual comparison of the frequency of individual calcium events displayed a right shift in both APP6 and APP9 astrocytes compared to WT conditions (Figure 2a,b). Further quantitative comparison of the frequency between WT and APP/PS1 astrocytes revealed significant differences between multiple groups. The average somatic calcium transients per minute were less frequent in WT6 compared to WT9 astrocytes (Figure 2c, one-way ANOVA, $F_{(3,525)} = 18.40$, $p < 0.0001$; Bonferroni's: WT6 ($n_t = 139$, $n_c = 37$, $n_s = 4$, $N = 3$) vs. WT9 ($n_t = 887$, $n_c = 154$, $n_s = 12$, $N = 4$), $p = 0.0293$), showing an effect of age. Similarly, calcium transients in APP6 astrocytes were less frequent compared to APP9 astrocytes (Figure 2c, one-way ANOVA, $F_{(3,525)} = 18.40$, $p < 0.0001$; Bonferroni's: APP6 ($n_t = 480$, $n_c = 84$, $n_s = 9$, $N = 3$) vs. APP9 ($n_t = 2{,}034$, $n_c = 253$, $n_s = 17$, $N = 5$), $p < 0.0001$). An additional effect of Aβ pathology was observed in APP9 astrocytes, as the calcium transient frequency was significantly increased in these astrocytes compared to WT9 astrocytes (Figure 2c, one-way ANOVA, $F_{(3,525)} = 18.40$, $p < 0.0001$; Bonferroni's: WT9 ($n_t = 887$, $n_c = 154$, $n_s = 12$, $N = 4$) vs. APP9 ($n_t = 2{,}034$, $n_c = 253$, $n_s = 17$, $N = 5$), $p < 0.0001$). This effect was further confirmed by analyzing the general activity levels of astrocytes in relation to aging and Aβ pathology by setting criteria for inactive (0 transients per minute), active (0 < 2 transients per minute), and hyperactive (> 2 transients per minute) astrocytes. APP9 astrocytes were significantly more hyperactive compared to WT9 astrocytes

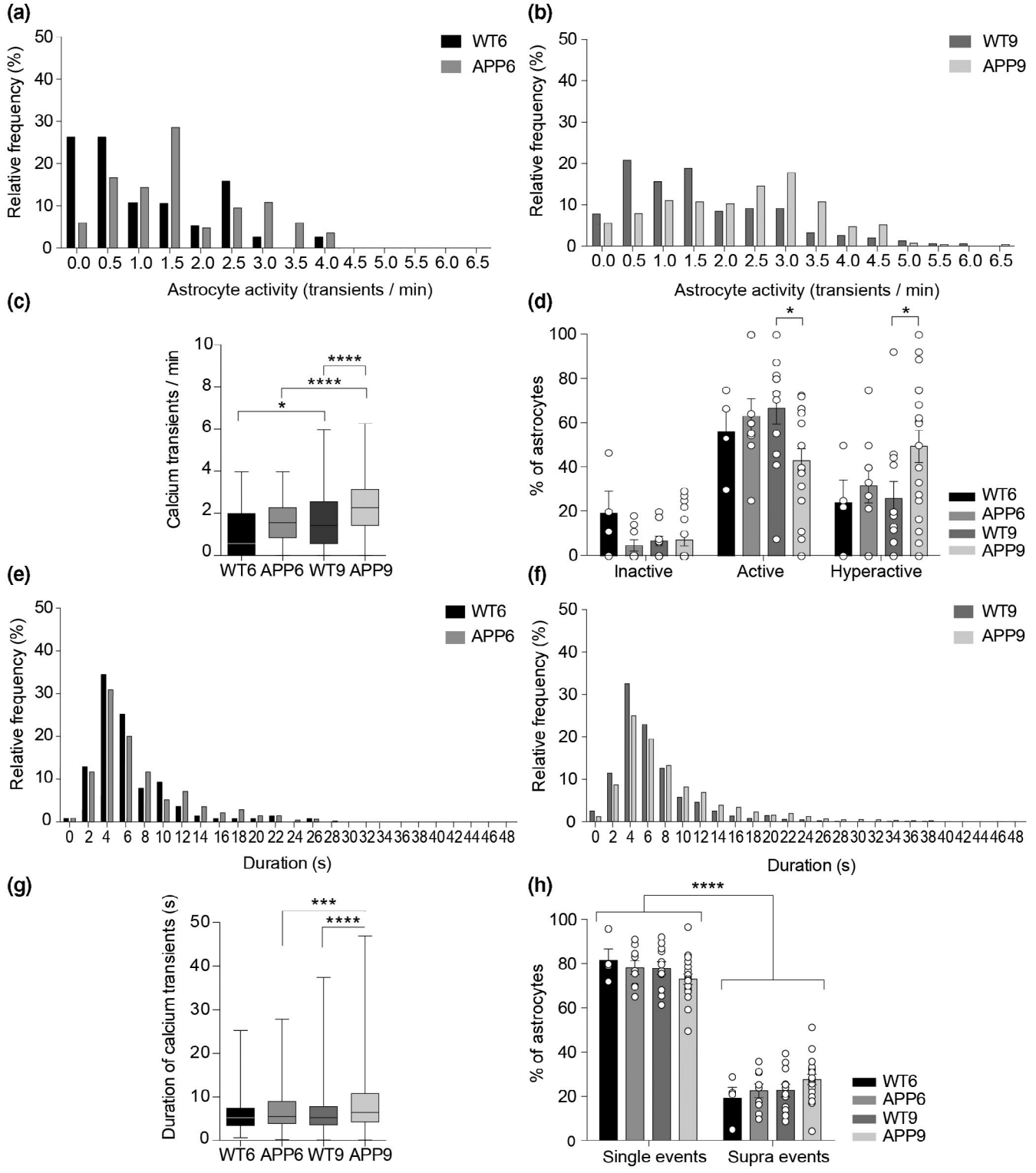

FIGURE 2 Calcium transients are more frequent and increase in duration as a result of aging and Aβ pathology. (a) Relative frequency of transients in WT6 and APP6 astrocytes. (b) Relative frequency of transients in WT9 and APP9 astrocytes. (c) The average frequency of transients for all groups. (d) Categorization of astrocytes as inactive (0 transients/min), active (0 < 2 transients/min), or hyperactive (> 2 transients/min). (e) Distribution of transient durations for WT6 and APP6. (f) Distribution of transient durations for WT9 and APP9. (g) The average duration of calcium transients for all groups. (h) The proportion of single events vs. supra-events for all groups. Data shown: WT6: $n_t = 139$, $n_c = 37$, $n_s = 4$, $N = 3$; APP6: $n_t = 480$, $n_c = 84$, $n_s = 9$, $N = 3$; WT9: $n_t = 887$, $n_c = 154$, $n_s = 12$, $N = 4$; APP9: $n_t = 2{,}034$, $n_c = 253$, $n_s = 17$, $N = 5$; $^*p \le 0.05$, $^{**}p \le 0.01$, $^{***}p \le 0.001$, $^{****}p \le 0.0001$. Boxplots indicate median, first and third quartiles, and min to max range

(Figure 2d, two-way ANOVA, group: $F_{(3,117)} = 4.054e^{-14}$, $p > 0.9999$; activity: $F_{(2,117)} = 38.21$, $p < 0.0001$; interaction: $F_{(6,117)} = 3.713$, $p = 0.0020$; Tukey's: WT9 ($n_t = 887$, $n_c = 154$, $n_s = 12$, $N = 4$) vs. APP9 ($n_t = 2{,}034$, $n_c = 253$, $n_s = 17$, $N = 5$), $p = 0.0243$) showing that Aβ pathology pushes astrocytes in the DG toward a more hyperactive phenotype (Figure 2d).

We next analyzed the duration of calcium transients between groups, as neuronal activity does not only affect calcium-wave frequency but also duration (Di Castro et al., 2011; Kanemaru et al., 2014; Schummers et al., 2008; Wu et al., 2014; reviewed by Bazargani & Attwell, 2016). Indeed, the duration of calcium transients was affected by both aging and Aβ pathology in our experiment. The distribution of astrocyte transient duration showed a right shift for both 6M and 9M APP/PS1 astrocytes compared to WT controls (Figure 2e,f). This effect was significant in APP9 astrocytes (Figure 2g, Kruskal–Wallis, $p < 0.0001$; Dunn's: WT6 ($n_t = 139$, $n_c = 37$, $n_s = 4$, $N = 3$) vs. APP6 ($n_t = 480$, $n_c = 84$, $n_s = 9$, $N = 3$), $p = 0.1880$; WT9 ($n_t = 887$, $n_c = 154$, $n_s = 12$, $N = 4$) vs. APP9 ($n_t = 2{,}034$, $n_c = 253$, $n_s = 17$, $N = 5$), $p < 0.0001$). The same analysis revealed an aging effect from APP6 to APP9 astrocytes (Figure 2g, Kruskal–Wallis, $p < 0.0001$; Dunn's: APP6 ($n_t = 480$, $n_c = 84$, $n_s = 9$, $N = 3$) vs. APP9 ($n_t = 2{,}034$, $n_c = 253$, $n_s = 17$, $N = 5$), $p = 0.0005$).

We further checked whether these changes in average transient duration were attributable to the duration of single events (single calcium transients) or supra-events (i.e., multiple single events within a larger transient). Analysis showed that single events occurred significantly more often compared to supra-events in every group (Figure 2h, two-way ANOVA, group: $F_{(3,39)} = 1.246$, $p = 0.3062$; event type: $F_{(1,39)} = 247.9$, $p < 0.0001$; interaction: $F_{(3,39)} = 1.288$, $p = 0.2920$). No additional effects were present indicating that the proportions between event subtypes were similar for WT6, WT9, APP6, and APP9 astrocytes.

Together, these data show that both aging and the presence of Aβ pathology changed the properties of somatic calcium transients in DG astrocytes.

3.2.1 | Aβ-plaque proximity does not affect astrocyte activity

We next determined whether astrocyte proximity to Aβ plaques was correlated with changes in somatic calcium-transient properties in the DG. Recorded astrocytes were divided into those proximal (≤ 80 μm) or distal (> 80 μm) from a visible Aβ plaque. Astrocytes recorded from APP/PS1 mouse brain slices without any visible Aβ plaques were classified as distal. Our data revealed no direct effect of Aβ-plaque proximity on either the frequency (Figure 3a, unpaired Student's t test, $t_{(82)} = 1.822$, $APP6_{prox}$ ($n_t = 153$, $n_c = 22$, $n_s = 9$, $N = 3$) vs. $APP6_{dis}$ ($n_t = 327$, $n_c = 62$, $n_s = 9$, $N = 3$), $p = 0.0722$; $t_{(251)} = 0.6401$, $APP9_{prox}$ ($n_t = 1140$, $n_c = 139$, $n_s = 17$, $N = 5$) vs. $APP9_{dis}$ ($n_t = 894$, $n_c = 114$, $n_s = 17$, $N = 5$), $p = 0.5227$) or the duration of calcium transients (Figure 3b, unpaired Student's t test, $t_{(478)} = 0.9041$, $APP6_{prox}$ ($n_t = 153$, $n_c = 22$, $n_s = 9$, $N = 3$) vs. $APP6_{dis}$ ($n_t = 327$, $n_c = 62$, $n_s = 9$, $N = 3$), $p = 0.3664$; Mann–Whitney, $APP9_{prox}$ ($n_t = 1140$, $n_c = 139$, $n_s = 17$, $N = 5$) vs. $APP9_{dis}$ ($n_t = 894$, $n_c = 114$, $n_s = 17$, $N = 5$), $p = 0.1984$). Further dividing astrocytes in inactive (0 events per minute), active (0 < 2 events per minute), and hyperactive (> 2 events per minute) subcategories revealed differences between groups. Although no significant differences were present between

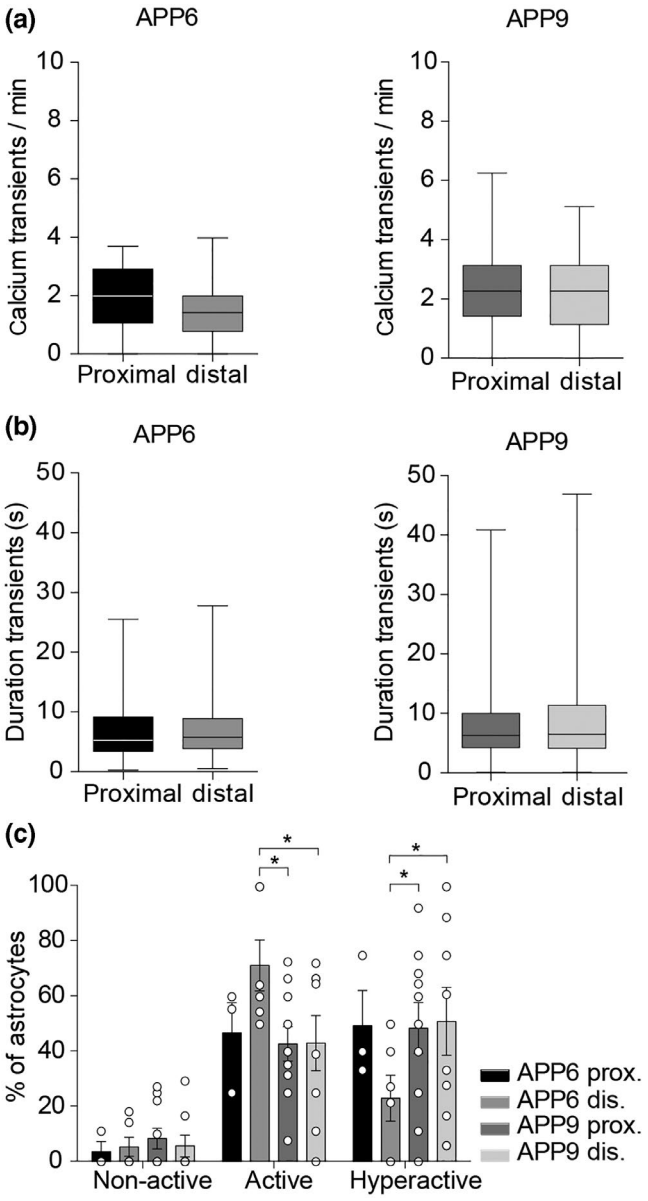

FIGURE 3 Plaque distance does not affect astrocyte activity in 6M and 9M APP/PS1 astrocytes. (a) Calcium transients per minute for APP/PS1 astrocytes located proximal (≤ 80 μm) or distal (> 80 μm) from aß plaques. (b) Calcium-transient duration for APP/PS1 astrocytes located proximal or distal from aß plaques. (c) Activity of astrocytes divided into inactive (0 transients/min), active (0 ≤ 2 transients/min), and hyperactive (2 > transients/min) for APP6 and APP9 astrocytes located proximal or distal from aß plaques. Data shown: $APP6_{prox}$: $n_t = 153$, $n_c = 22$, $n_s = 9$, $N = 3$; $APP6_{dis}$: $n_t = 327$, $n_c = 62$, $n_s = 9$, $N = 3$; $APP9_{prox}$: $n_t = 1140$, $n_c = 139$, $n_s = 17$, $N = 5$; $APP9_{dis}$: $n_t = 894$, $n_c = 114$, $n_s = 17$, $N = 5$; $^*p \leq 0.05$. Boxplots indicate median, first and third quartiles, and min to max range

proximal and distal astrocytes within groups, less proximal and distal APP9 astrocytes were active compared to distal APP6 astrocytes (Figure 3c, two-way ANOVA, group: $F_{(3,23)} = 0$, $p > 0.9999$; activity: $F_{(2,46)} = 17.15$, $p < 0.0001$; interaction: $F_{(6,46)} = 1.568$, $p = 0.1780$; Fisher's LSD, $APP6_{dis}$ ($n_t = 327$, $n_c = 62$, $n_s = 9$, $N = 3$) vs. $APP9_{prox}$ ($n_t = 1140$, $n_c = 139$, $n_s = 17$, $N = 5$), $p = 0.0158$; $APP6_{dis}$ ($n_t = 327$, $n_c = 62$, $n_s = 9$, $N = 3$) vs. $APP9_{dis}$ ($n_t = 894$, $n_c = 114$, $n_s = 17$, $N = 5$), $p = 0.0221$). Vice versa, significantly more proximal and distal APP9 astrocytes were hyperactive compared to distal APP6 astrocytes (Figure 3c, two-way ANOVA, group: $F_{(3,23)} = 0$, $p > 0.9999$; activity: $F_{(2,46)} = 17.15$, $p < 0.0001$; interaction: $F_{(6,46)} = 1.568$, $p = 0.1780$; Fisher's LSD, $APP6_{dis}$ ($n_t = 327$, $n_c = 62$, $n_s = 9$, $N = 3$) vs. $APP9_{prox}$ ($n_t = 1140$, $n_c = 139$, $n_s = 17$, $N = 5$), $p = 0.0304$; $APP6_{dis}$ ($n_t = 327$, $n_c = 62$, $n_s = 9$, $N = 3$) vs. $APP9_{dis}$ ($n_t = 894$, $n_c = 114$, $n_s = 17$, $N = 5$), $p = 0.0237$). Together, these data suggest that astrocytes increase their activity with age and progressive Aβ pathology but do not indicate an effect of Aβ-plaque proximity.

3.3 | Efficiency of astrocyte calcium-wave initiation and propagation is increased in 9M astrocytes

The extent and the efficiency of astrocyte coupling in a syncytium contribute to the effectiveness of astrocytes to regulate neuronal activity (Wallraff et al., 2006). To determine whether astrocyte-network activity is changed due to aging or Aβ pathology, we analyzed the efficiency with which a calcium event is propagated throughout the astrocyte syncytium. We quantified the average number of astrocyte pairs, the number of events per astrocyte pair, the number of astrocytes capable of initiating a wave containing *x* astrocytes, and the number of astrocytes in a calcium wave. To control for a difference in the average number of astrocytes per slice between the groups (Figure S1), we quantified the number of astrocyte pairs as a percentage of the total number of possible astrocyte pairs. The total number of possible astrocyte pairs in a slice was defined as all combinations of astrocytes that were no more than 50 μm apart and showed transients between 0.5 and 3 s from each other (Delekate et al., 2014; Oberheim et al., 2009).

The initial analysis showed that the percentage of astrocyte pairs did not differ significantly between the groups (Figure 4a), suggesting that each group contained relatively an equal number of connected astrocytes. To confirm the absence of an aging effect, we additionally pooled the WT and APP/PS1 groups per age category (Figure 4b), showing that the number of astrocyte pairs is neither affected by Aβ pathology nor by aging. We additionally assessed the average number of events per astrocyte pair and showed that also astrocyte-pair activity is similar for all groups (Figure 4c,d). Subsequently, we were interested in whether some astrocytes were more likely to initiate calcium waves than others. Therefore, we quantified the average number of unique seeds per brain slice for each group. A unique seed was defined as an individual astrocyte that was capable of initiating a calcium wave through ≥ 3 astrocytes. Aβ pathology did not change the number of unique seeds per brain slice between genotypes (Figure 4e). This was further confirmed by pooling the seed astrocytes over all waves (Figure 4f). Interestingly, we observed an aging effect (Figure 4e). In particular, APP9 astrocytes were significantly more likely to initiate a three- and four-astrocyte wave compared to APP6 astrocytes (Figure 4e, two-way ANOVA, group: $F_{(3,38)} = 2.441$, $p = 0.0791$; astrocytes in wave: $F_{(5,190)} = 17.88$, $p < 0.0001$; interaction: $F_{(15,190)} = 0.7612$, $p = 0.7191$; Tukey's: APP6 ($n_s = 9$, $N = 3$) vs. APP9 ($n_s = 17$, $N = 5$) - three astrocytes, $p = 0.0194$; four astrocytes, $p = 0.0411$). Pooling the data per age category confirmed this aging effect (Figure 4g, two-way ANOVA, group: $F_{(1,40)} = 5.719$, $p = 0.0216$; astrocytes in wave: $F_{(5,200)} = 20.56$, $p < 0.0001$; interaction: $F_{(5,200)} = 2.286$, $p = 0.0476$; Tukey's: 6M ($n_s = 13$, $N = 6$) vs. 9M ($n_s = 29$, $N = 9$) - three astrocytes, $p = 0.0149$; four astrocytes, $p = 0.0207$). This aging effect between 6M and 9M astrocytes was not confirmed when all waves were pooled (Figure 4h, Mann–Whitney, 6M ($n_s = 13$, $N = 6$) vs. 9M ($n_s = 29$, $N = 9$), $p = 0.06$).

Although there was a significant difference between WT6 and APP9 astrocytes on the percentage of three-astrocyte waves (Figure 4i, two-way ANOVA, group: $F_{(3,38)} = 0.4442$, $p = 0.7228$; astrocytes in wave: $F_{(5,190)} = 18.77$, $p < 0.0001$; interaction: $F_{(15,190)} = 1.291$, $p = 0.2112$; Tukey's: WT6 ($n_s = 4$, $N = 3$) vs. APP9 ($n_s = 17$, $N = 5$) - three-astrocyte waves, $p = 0.0041$), neither genotype nor age had a substantial effect on the number of astrocytes in a calcium wave (Figure 4i,j). Yet, the 6M astrocytes overall seemed to be less capable of initiating waves containing a high number of astrocytes (≥ 5 astrocytes) and showed overall fewer waves containing a high number of astrocytes (Figure 4g,j). We therefore performed calcium-wave analysis specifically for waves containing ≥ 5 astrocytes (Figure 5). Whereas no significant effect of the genotype was present (Figure 5a,c), pooling the data per age category confirmed that 9M astrocytes are significantly more capable of initiating and propagating waves that contained a high number of astrocytes (Figure 5b, Mann–Whitney, 6M ($n_s = 13$, $N = 6$) vs. 9M ($n_s = 29$, $N = 9$), $p = 0.0288$; Figure 5d, Mann–Whitney, 6M ($n_s = 13$, $N = 6$) vs. 9M ($n_s = 29$, $N = 9$), $p = 0.0366$).

Together, these data suggest that aging rather than Aβ pathology affects the extent and efficiency with which astrocytes form spontaneous sequential calcium events.

3.4 | Increased efficiency of astrocyte calcium-wave initiation and propagation is not unique for 9M astrocytes

We next determined with a null-model approach (Farine, 2017) whether the increase in the number of waves containing a high number of astrocytes was unique for the 9M astrocytes or whether co-occurrence of individual astrocyte calcium transients happened by chance (Figure 6a). The astrocyte network parameters that we tested were the percentage of astrocytes capable of initiating a wave containing ≥ 5 astrocytes, the percentage of waves containing

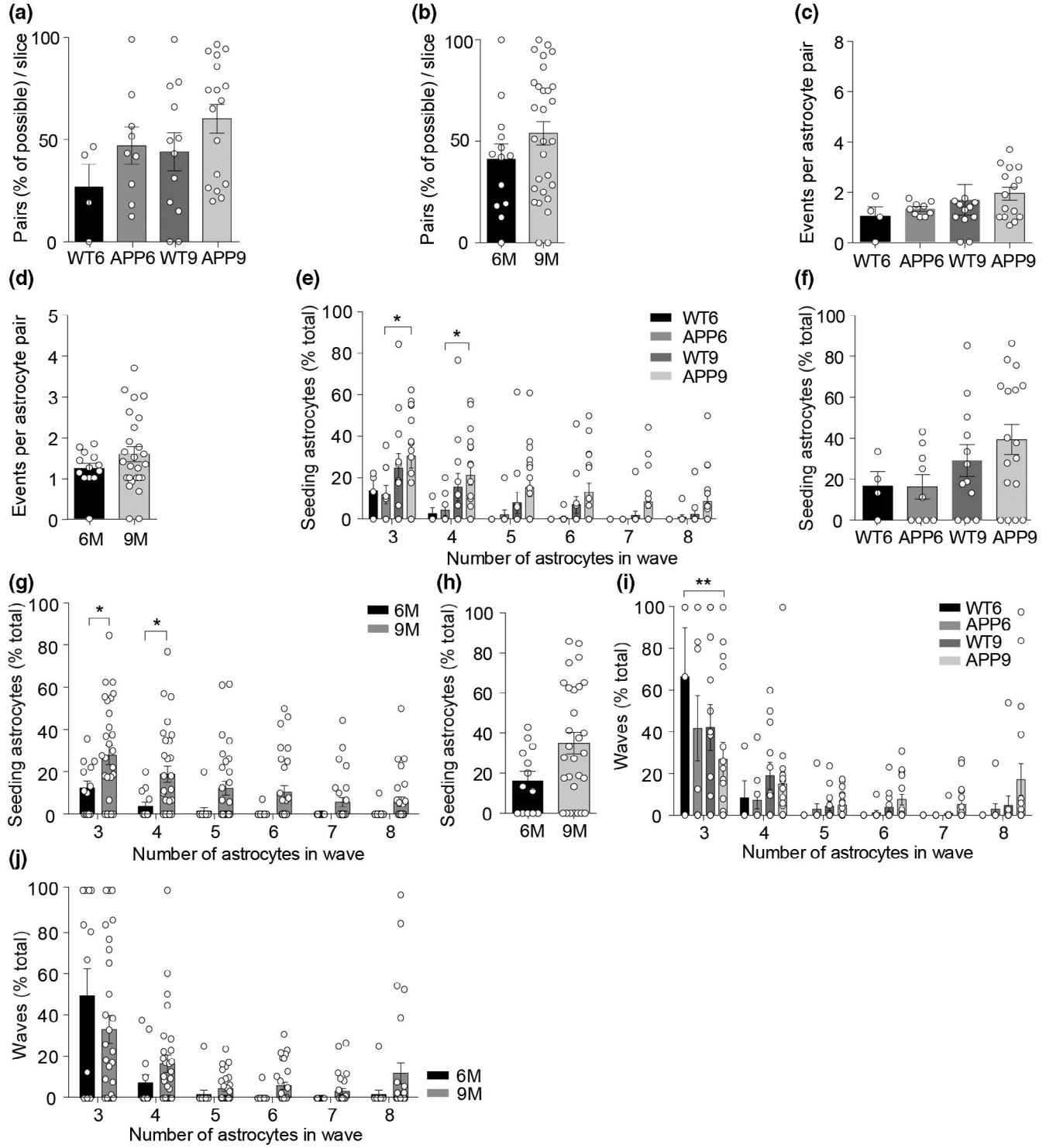

FIGURE 4 The effect of aging and Aβ pathology on calcium-wave initiation and propagation. (a,b) Astrocyte pairs present as percentage of total possible number of astrocyte pairs for all groups and combined 6M and 9M astrocyte data. (c,d) Average number of paired events per astrocyte pair for all groups separately and combined 6M and 9M astrocyte data. (e) Percentage of astrocytes capable of initiating a wave containing "*x*" number of astrocytes for all groups. (f) Percentage of astrocytes capable of initiating a wave for all groups. (g) Percentage of astrocytes capable of initiating a wave containing "*x*" number of astrocytes for combined 6M and 9M astrocyte data. (h) Percentage of astrocytes capable of initiating a wave for combined 6M and 9M astrocyte data. (i) Percentage of waves containing "*x*" number of astrocytes for all groups. (j) Percentage of waves containing "*x*" number of astrocytes for pooled 6M and 9M astrocyte data. Data shown: WT6: $n_s = 4$, $N = 3$; APP6: $n_s = 9$, $N = 3$; WT9: $n_s = 12$, $N = 4$; and APP9: $n_s = 17$, $N = 5$; $^*p \leq 0.05$, $^{**}p \leq 0.01$

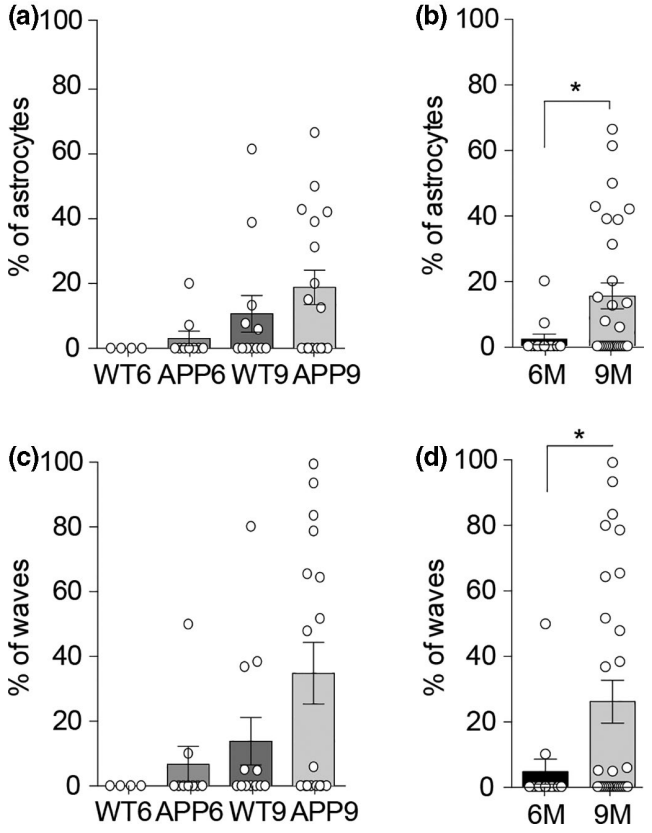

FIGURE 5 Calcium waves containing a high number of astrocytes are more likely to be initiated and occur more often in 9M astrocytes. (a) Percentage of astrocytes (unique seeds) capable of initiating a wave containing ≥ 5 astrocytes for all groups. (b) Percentage of astrocytes (unique seeds) capable of initiating a wave containing ≥ 5 astrocytes for combined 6M and 9M astrocyte data. (c) Percentage of waves containing ≥ 5 astrocytes for all groups. (d) Percentage of waves containing ≥ 5 astrocytes for pooled 6M and 9M astrocyte data. Data shown: WT6: $n_s = 4$, $N = 3$; APP6: $n_s = 9$, $N = 3$; WT9: $n_s = 12$, $N = 4$; and APP9: $n_s = 17$, $N = 5$; $^*p \leq 0.05$

a high number of astrocytes, and the number of events per astrocyte pair. The observed values for all three parameters fell within the 95% interval of the Gaussian distribution we obtained by performing calcium-wave analysis on the generated null models (Figure 6b–d). This suggests that the observation that 9M astrocytes show increased efficiency of calcium-wave initiation and propagation compared to 6M astrocytes is not unique to 9M astrocytes and does not significantly differ from what you would expect based on chance, taking into account the number of individual astrocyte events recorded in this group.

Altogether, the data presented in this study indicate that calcium signaling in individual astrocytes is to a large extent subject to aging, characterized by an increased calcium transient frequency and duration in 9M astrocytes versus 6M astrocytes. Moreover, it shows that this effect of aging is reinforced by the presence of Aβ pathology, as additional differences in calcium transient frequency and duration were found between 9M WT and 9M APP/PS1 astrocytes. Our data additionally reveal no effect of Aβ-plaque proximity on astrocyte calcium signaling in *ex-vivo* conditions. The calcium changes in individual astrocytes did not lead to a physiological change in astrocyte network activity.

4 | DISCUSSION

Despite all fundamental research into AD over the last decades, there remains a gap in our understanding of the mechanisms underlying the cascade of events that ultimately lead to dementia and AD. Over the years, the contribution of astrocytes to proper neuronal functioning in the healthy brain, as well as their role in pathophysiology, has become increasingly clear (reviewed by Osborn et al., 2016; Pekny et al., 2016; Santello et al., 2019; Verkhratsky & Nedergaard, 2018). As such, it is now widely accepted that astrocyte calcium signaling is important for the physiological functioning of astrocytes and their regulatory role in neuronal physiology. Various studies have shown that aberrant calcium signaling in astrocytes contributes to the pathology of neurodegenerative diseases, including AD (Demuro et al., 2005; Isaacs et al., 2006; Kanemaru et al., 2013; Stutzmann, 2006; reviewed by Stutzmann, 2007). Nevertheless, exactly how astrocyte calcium signaling is affected throughout AD progression is still unclear. The focus of this study is to understand how Aβ pathology affects calcium signaling in astrocytes throughout AD progression. We characterized calcium signaling properties of $GCaMP3^+/SR101^+$ astrocytes in hippocampal slices containing the DG of 6M and 9M APP/PS1 mice. Moreover, we studied whether and how these properties are affected by Aβ-plaque proximity. Our findings demonstrate that calcium signaling in individual DG astrocytes is affected by Aβ pathology and that these effects are substantially reinforced by aging. Although minor effects were present in 6M APP/PS1 astrocytes, the impact of Aβ pathology on calcium signaling properties were clearly present in 9M APP/PS1 astrocytes. Moreover, our data revealed a main effect of aging, rather than an effect of Aβ-plaque pathology. Further analysis using both the observed and a pseudo-randomized data set revealed that our initially observed effect on astrocyte network activity is at chance level.

Our initial analysis focused on the properties of calcium signals in individual astrocytes in the DG of hippocampal slices in 6M and 9M APP/PS1 mice. Our findings largely corroborate with earlier observations in cortical astrocytes of 6M and 9M AD model mice *in vivo*. Similar to our results, cortical astrocytes in APPPS1-21 and APP/PS1 mice show an increase in spontaneous calcium transient frequency (Delekate et al., 2014; Kuchibhotla et al., 2009). Although clearly present in 9M APP/PS1 astrocytes, this effect did not reach significance when comparing the 6M age groups, probably due to high intragroup variability. Although not significant, 6M APP/PS1 astrocytes displaying signs of increased calcium activity corresponds to studies indicating that Aβ pathology starts with the accumulation of specifically earlier forms of Aβ, that is Aβ oligomers that progressively affect the physiological function of neurons and glia cells in AD progression (DaRocha-Souto et al., 2011; Hsia et al., 1999; Lambert et al., 1998; Li et al., 2009; reviewed by Selkoe & Hardy, 2016). Moreover, Aβ

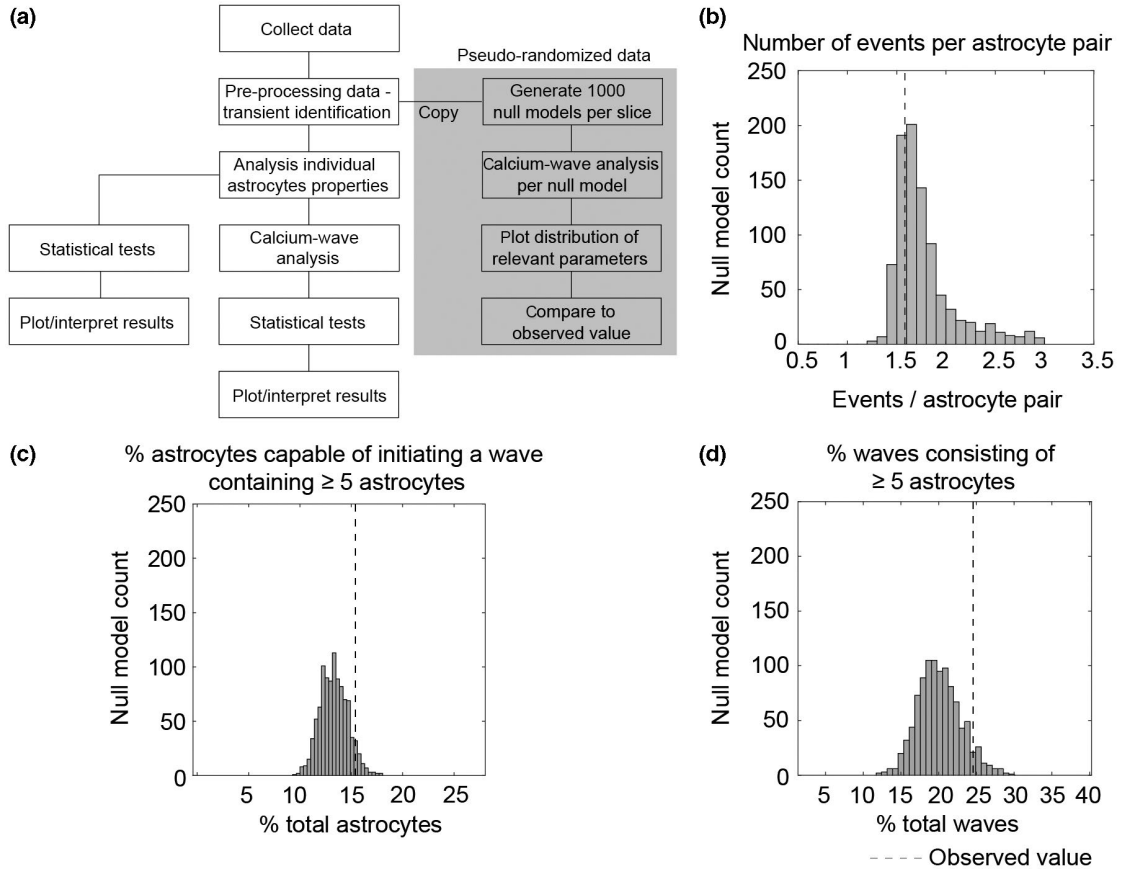

FIGURE 6 Increased efficiency of calcium-wave initiation and propagation is not unique for 9M astrocytes. (a) Overview of null-model approach. A total of 1,000 pseudo-randomized null models were generated per brain slice using the observed data of 9M brain slices. Each plot indicates the group distribution obtained from a total of 29,000 null models; 29 slices, 1,000 null models per slice. The obtained distributions for relevant parameters were compared to observed values. (b) Plot showing the null-model distribution of values indicating the average number of events per astrocyte pair for 9M astrocytes. Dashed line indicates average value as observed in Figure 4d. (c) Plot showing the null-model distribution of values indicating the percentage of astrocytes capable of initiating a wave containing ≥ 5 astrocytes. Dashed line indicates average value as observed in Figure 5b. (d) Plot showing the null-model distribution of values indicating the percentage of waves containing ≥ 5 astrocytes. Dashed line indicates average value as observed in Figure 5d

oligomers can directly increase calcium concentrations and spontaneous calcium activity in cortical and hippocampal astrocytes, both *in vivo* (Arbel-Ornath et al., 2017) and *ex-vivo* (Abramov et al., 2003; Bosson et al., 2017; Tyurikova et al., 2018). In contrast to our results, previous research detected no differences in the duration of spontaneous calcium transients between WT and APPPS1-21 astrocytes (Delekate et al., 2014). This disparity could be the result of age differences since previous studies made no distinction between 6M and 9M AD mouse model astrocytes but instead pooled astrocytes within a range from 6M to 9M (Delekate et al., 2014; Kuchibhotla et al., 2009). Indeed, the effect on calcium transient duration in our data was mainly present in 9M APP/PS1 astrocytes, and we found that the properties of 6M APP/PS1 astrocytes are still very similar to those of healthy age-matched controls. This is in contrast to an *in-vivo* study in which cortical astrocytes in prepathological stages of AD progression in Tg2576, 3xTG-AD and APPSwDI mice already showed increased spontaneous calcium activity compared to control astrocytes (Takano et al., 2007). Differences between mouse models and *in-vivo* and *ex-vivo* conditions may underlie these contrasting observations. For example, *ex-vivo* slice preparations remove cells from their three-dimensional context which may affect their physiological properties. *In-vivo* and *ex-vivo* conditions may therefore not be directly comparable, and the results presented in this study apply solely to *ex-vivo* conditions. This is also true for assessing the effect of Aβ-plaque proximity, as the reduced dimensionality of our data may have contributed to the false classification of astrocytes as distal. Moreover, the 290 μm slice thickness allowed for the presence of Aβ plaques in deeper layers of the slice, which were difficult to identify using our experimental approach. Therefore, we cannot draw any definitive conclusions on the effect that Aβ-plaque proximity exerts on astrocyte activity.

Another observation from our results is that calcium signaling in astrocytes is to a large extent affected by aging, as calcium transient frequency and duration were significantly altered between both WT6 and WT9 astrocytes and between APP6 and APP9 astrocytes. Also, overall, more 9M astrocytes were hyperactive compared to 6M astrocytes. The GFAP promoter driving GCaMP3 expression becomes more active with increasing astrocyte reactivity and age

and can be leaky (reviewed by Brenner & Messing, 2021), causing GCaMP3 to be increasingly expressed, also by cell types other than astrocytes. We increased the probability of the analyzed fluorescence signals being astrocyte specific by labeling astrocytes with the astrocyte-specific dye SR101. The efficacy of SR101 is however dependent on specific conditions and can therefore not be considered a gold-standard marker (Nimmerjahn & Helmchen, 2012). Although we further ensured astrocyte specificity by filtering fluorescence signals based on their temporal resolution, the possibility that cells other than astrocytes were included in the analyses should be taken into account when interpreting our results. The possibility that GCaMP3 expression levels have further affected the frequency or duration of individual calcium transients is unlikely considering the fast kinetics of GCaMP3 relative to the multi-second scale of somatic astrocyte calcium transients (Tian et al., 2009). An additional effect of GCaMP3 expression on the number of astrocytes detected during recordings was minimized by solely using astrocyte percentages rather than absolute counts. A likely explanation is therefore that fluctuations in astrocyte calcium concentration increase with age, introducing an aging effect in our data. Nevertheless, as our data are two-dimensional and of limited resolution, it is important to consider that this conclusion only applies to somatic calcium transients. Whether a similar effect is present on local calcium transients (reviewed by Semyanov et al., 2020), for example in astrocyte microdomains, remains subject to further research.

In addition to characterizing calcium signaling properties of individual astrocytes, we performed astrocyte network analyses to find out whether the functional connectivity between astrocytes was affected by either age or Aβ pathology. The initiation and propagation of multi-astrocyte calcium waves were observed in all groups in DG astrocytes in *ex-vivo* hippocampal slices. This observation is in contrast to previous studies where no spontaneous waves were detected in WT astrocytes using an *in-vivo* imaging approach to record calcium transients in cortical astrocytes (Delekate et al., 2014; Kuchibhotla et al., 2009). The fact that *ex-vivo* slice preparations induce astrocyte reactivity and affect WT astrocytes could account for these results (Takano et al., 2014). Alternatively, it might be that DG astrocytes respond differently to experimental conditions compared to cortical astrocytes as used in Kuchibhotla et al. (2009) and Delekate et al. (2014). Regarding astrocyte network parameters, we did neither observe a significant effect of Aβ pathology on the number of astrocyte pairs nor on the number of calcium events generated by these astrocyte pairs. The same is true for the number of astrocytes capable of initiating calcium waves and the number of astrocytes that participated in a calcium wave. Nevertheless, the 9M astrocytes displayed a significantly increased efficiency of initiation and propagation of calcium waves with ≥ 5 astrocytes compared to 6M astrocytes. This could be due to changes in general calcium concentrations or alteration in the molecular profile of astrocytes. We and others have shown that aged astrocytes have a more inflammatory and active phenotype (Clarke et al., 2018; Orre et al., 2014).

To ensure that these astrocyte network patterns observed in 9M astrocytes have a physiological basis and are not based on chance processes, we performed additional network analysis using a null-model approach (Farine, 2017). An approach like this is especially preferred when analyzing interaction data obtained from a network of individual entities, in our case astrocytes. The aim of using a null-model approach was therefore to assess whether the astrocyte network patterns observed in our data were unique for the 9M astrocytes we recorded from. To our surprise, comparing observed astrocyte network parameters to results we obtained from null-model analysis indicates that the effects we found are not significantly different from what you would expect based on chance when taking into account the number of individual events in 9M astrocytes. That is, the observation that 9M astrocytes show increased efficiency of calcium wave initiation and propagation compared to 6M astrocytes is based on chance, primarily caused by the high number of individual astrocyte events generated in the 9M astrocyte group. This also means that we cannot conclude that calcium transients of individual astrocytes observed in our data are causally related, that is based on our analysis it is most likely that individual events manifested as a wave-like phenomenon by chance. This, however, does not affect our earlier conclusion that both aging and Aβ pathology alter calcium transient frequency and duration since these data were obtained from individual astrocytes. Nevertheless, interaction data from other studies similar to the data presented here should be interpreted with caution when no additional null-model analyses are performed.

Together, we show that the frequency and duration of calcium transients is subject to Aβ pathology and increases with age in individual DG astrocytes in hippocampal *ex-vivo* slices. In addition, we show that astrocyte network patterns in 9M astrocytes observed in this study most likely have no physiological basis but are instead based on chance, illustrating the importance of using null models for astrocyte network analysis. With these results in mind, future research is needed to further look into how deregulation of specifically individual astrocyte activity affects neuronal functioning in relation to AD and aging. Taken together, the data in this study aid the understanding of astrocyte pathophysiology in the DG following exposure to Aβ pathology and suggest that AD onset does not induce significant changes in astrocyte activity. More advanced Aβ pathology, however, does impact astrocyte activity, which may act as a compensatory change to ameliorate disease progression.

DECLARATION OF TRANSPARENCY

The authors, reviewers and editors affirm that in accordance to the policies set by the *Journal of Neuroscience Research*, this manuscript presents an accurate and transparent account of the study being reported and that all critical details describing the methods and results are present.

ACKNOWLEDGMENTS

This work was supported by the University of Amsterdam (LMO, NLMC) and ZonMW 733050816 (CFMH, EMH) - The ZonMw, Dementia Research and Innovation Program “Memorabel.”

CONFLICT OF INTEREST

The authors declare no conflict of interest.

AUTHOR CONTRIBUTIONS

Conceptualization, N.L.M.C. and E.M.H.; *Methodology*, C.F.M.H., L.M.O., N.L.M.C., and E.M.H.; *Investigation*, C.F.M.H. and L.M.O.; *Formal Analysis*, C.F.M.H. and L.M.O.; *Software*, C.F.M.H., L.M.O., and N.L.M.C.; *Visualization*, L.M.O. and C.F.M.H.; *Writing – Original Draft*, L.M.O. and C.F.M.H.; *Writing – Review & Editing*, C.F.M.H., N.L.M.C., and E.M.H.; *Supervision*, N.L.M.C. and E.M.H.; *Funding Acquisition*, E.M.H.

PEER REVIEW

The peer review history for this article is available at https://publons.com/publon/10.1002/jnr.25042.

DATA AVAILABILITY STATEMENT

All data are available upon reasonable request to e.m.hol-2@umcutrecht.nl.

ORCID

Christiaan F. M. Huffels https://orcid.org/0000-0002-9070-3644
Lana M. Osborn https://orcid.org/0000-0002-5900-0246
Natalie L. M. Cappaert https://orcid.org/0000-0002-1292-9517
Elly M. Hol https://orcid.org/0000-0001-5604-2603

REFERENCES

Abramov, A. Y., Canevari, L., & Duchen, M. R. (2003). Changes in intracellular calcium and glutathione in astrocytes as the primary mechanism of amyloid neurotoxicity. *Journal of Neuroscience*, *23*(12), 5088–5095. https://doi.org/10.1523/JNEUROSCI.23-12-05088.2003

Arbel-Ornath, M., Hudry, E., Boivin, J. R., Hashimoto, T., Takeda, S., Kuchibhotla, K. V., Hou, S., Lattarulo, C. R., Belcher, A. M., Shakerdge, N., Trujillo, P. B., Muzikansky, A., Betensky, R. A., Hyman, B. T., & Bacskai, B. J. (2017). Soluble oligomeric amyloid-β induces calcium dyshomeostasis that precedes synapse loss in the living mouse brain. *Molecular Neurodegeneration*, *12*(1), 27. https://doi.org/10.1186/s13024-017-0169-9

Balkenius, A., Johansson, A. J., & Balkenius, C. (2015). Comparing analysis methods in functional calcium imaging of the insect brain. *PLoS ONE*, *10*(6), e0129614. https://doi.org/10.1371/journal.pone.0129614

Bazargani, N., & Attwell, D. (2016). Astrocyte calcium signaling: The third wave. *Nature Neuroscience*, *19*(2), 182–189. https://doi.org/10.1038/nn.4201

Bertoni-Freddari, C., Fattoretti, P., Solazzi, M., Giorgetti, B., Di Stefano, G., Casoli, T., & Meier-Ruge, W. (2003). Neuronal death versus synaptic pathology in Alzheimer's disease. *Annals of the New York Academy of Sciences*, *1010*, 635–638. https://doi.org/10.1196/annals.1299.116

Bosson, A., Paumier, A., Boisseau, S., Jacquier-Sarlin, M., Buisson, A., & Albrieux, M. (2017). TRPA1 channels promote astrocytic Ca(2+) hyperactivity and synaptic dysfunction mediated by oligomeric forms of amyloid-β peptide. *Molecular Neurodegeneration*, *12*(1), 53. https://doi.org/10.1186/s13024-017-0194-8

Braak, H., & Braak, E. (1991). Neuropathological stageing of Alzheimer-related changes. *Acta Neuropathologica*, *82*(4), 239–259. https://doi.org/10.1007/BF00308809

Braak, H., & Braak, E. (1996). Evolution of the neuropathology of Alzheimer's disease. *Acta Neurologica Scandinavica*, *94*(S165), 3–12. https://doi.org/10.1111/j.1600-0404.1996.tb05866.x

Braak, H., Braak, E., Yilmazer, D., de Vos, R. A., Jansen, E. N., & Bohl, J. (1996). Pattern of brain destruction in Parkinson's and Alzheimer's diseases. *Journal of Neural Transmission*, *103*(4), 455–490. https://doi.org/10.1007/BF01276421

Brenner, M., & Messing, A. (2021). Regulation of GFAP expression. *ASN Neuro*, *13*, 175909142098120. https://doi.org/10.1177/17590914209812 06

Clarke, L. E., Liddelow, S. A., Chakraborty, C., Münch, A. E., Heiman, M., & Barres, B. A. (2018). Normal aging induces A1-like astrocyte reactivity. *Proceedings of the National Academy of Sciences of the United States of America*, *115*(8), E1896–E1905. https://doi.org/10.1073/pnas.1800165115

Cornell-Bell, A. H., Finkbeiner, S. M., Cooper, M. S., & Smith, S. J. (1990). Glutamate induces calcium waves in cultured astrocytes: Long-range glial signaling. *Science*, *247*(4941), 470–473. https://doi.org/10.1126/science.1967852

DaRocha-Souto, B., Scotton, T. C., Coma, M., Serrano-Pozo, A., Hashimoto, T., Sereno, L., Rodrıguez, M., Sanchez, B., Hyman, B. T., & Gomez-Isla, T. (2011). Brain oligomeric A-amyloid but not total amyloid plaque burden correlates with neuronal loss and astrocyte inflammatory response in amyloid precursor protein/tau transgenic mice. *Journal of Neuropathology and Experimental Neurology*, *70*(5), 17–376. https://doi.org/10.1097/NEN.0b013e318217a118

Delekate, A., Füchtemeier, M., Schumacher, T., Ulbrich, C., Foddis, M., & Petzold, G. C. (2014). Metabotropic P2Y1 receptor signalling mediates astrocytic hyperactivity in vivo in an Alzheimer's disease mouse model. *Nature Communications*, *5*, 5422. https://doi.org/10.1038/ncomms6422

Demuro, A., Mina, E., Kayed, R., Milton, S. C., Parker, I., & Glabe, C. G. (2005). Calcium Dysregulation and membrane disruption as a ubiquitous neurotoxic mechanism of soluble amyloid oligomers. *Journal of Biological Chemistry*, *280*(17), 17294–17300. https://doi.org/10.1074/jbc.M500997200

Di Castro, M. A., Chuquet, J., Liaudet, N., Bhaukaurally, K., Santello, M., Bouvier, D., Tiret, P., & Volterra, A. (2011). Local Ca^{2+} detection and modulation of synaptic release by astrocytes. *Nature Neuroscience*, *14*(10), 1276–1284. https://doi.org/10.1038/nn.2929

Diedrich, J., Wietgrefe, S., Zupancic, M., Staskus, K., Retzel, E., Haase, A. T., & Race, R. (1987). The molecular pathogenesis of astrogliosis in scrapie and Alzheimer's disease. *Microbial Pathogenesis*, *2*(6), 435–442. https://doi.org/10.1016/0882-4010(87)90050-7

Eng, L. F., Vanderhaeghen, J. J., Bignami, A., & Gerstl, B. (1971). An acidic protein isolated from fibrous astrocytes. *Brain Research*, *28*(2), 351–354. https://doi.org/10.1016/0006-8993(71)90668-8

Escartin, C., Galea, E., Lakatos, A., O'Callaghan, J. P., Petzold, G. C., Serrano-Pozo, A., Steinhäuser, C., Volterra, A., Carmignoto, G., Agarwal, A., Allen, N. J., Araque, A., Barbeito, L., Barzilai, A., Bergles, D. E., Bonvento, G., Butt, A. M., Chen, W.-T., Cohen-Salmon, M., … Verkhratsky, A. (2021). Reactive astrocyte nomenclature, definitions, and future directions. *Nature Neuroscience*, *24*(3), 312–325. https://doi.org/10.1038/s41593-020-00783-4

Farine, D. R. (2017). A guide to null models for animal social network analysis. *Methods in Ecology and Evolution*, *8*(10), 1309–1320. https://doi.org/10.1111/2041-210X.12772

Hol, E. M., & Pekny, M. (2015). Glial fibrillary acidic protein (GFAP) and the astrocyte intermediate filament system in diseases of the central nervous system. *Current Opinion in Cell Biology*, *32*, 121–130. https://doi.org/10.1016/j.ceb.2015.02.004

Hsia, A. Y., Masliah, E., McConlogue, L., Yu, G.-Q., Tatsuno, G., Hu, K., Kholodenko, D., Malenka, R. C., Nicoll, R. A., & Mucke, L. (1999). Plaque-independent disruption of neural circuits in Alzheimer's disease mouse models. *Proceedings of the National Academy of Sciences of the Unites States of America*, *96*(6), 3228–3233. https://doi.org/10.1073/pnas.96.6.3228

Isaacs, A. M., Senn, D. B., Yuan, M., Shine, J. P., & Yankner, B. A. (2006). Acceleration of amyloid β-peptide aggregation by physiological concentrations of calcium. *Journal of Biological Chemistry*, *281*(38), 27916–27923. https://doi.org/10.1074/jbc.M602061200

Jankowsky, J. L., Fadale, D. J., Anderson, J., Xu, G. M., Gonzales, V., Jenkins, N. A., Copeland, N. G., Lee, M. K., Younkin, L. H., Wagner, S. L., Younkin, S. G., & Borchelt, D. R. (2004). Mutant presenilins specifically elevate the levels of the 42 residue beta-amyloid peptide in vivo: Evidence for augmentation of a 42-specific gamma secretase. *Human Molecular Genetics*, *13*(2), 159–170. https://doi.org/10.1093/hmg/ddh019

Kafitz, K. W., Meier, S. D., Stephan, J., & Rose, C. R. (2008). Developmental profile and properties of sulforhodamine 101—Labeled glial cells in acute brain slices of rat hippocampus. *Journal of Neuroscience Methods*, *169*(1), 84–92. https://doi.org/10.1016/j.jneumeth.2007.11.022

Kamphuis, W., Middeldorp, J., Kooijman, L., Sluijs, J. A., Kooi, E.-J., Moeton, M., Freriks, M., Mizee, M. R., & Hol, E. M. (2014). Glial fibrillary acidic protein isoform expression in plaque related astrogliosis in Alzheimer's disease. *Neurobiology of Aging*, *35*(3), 492–510. https://doi.org/10.1016/j.neurobiolaging.2013.09.035

Kamphuis, W., Orre, M., Kooijman, L., Dahmen, M., & Hol, E. M. (2012). Differential cell proliferation in the cortex of the APPswePS1dE9 Alzheimer's disease mouse model. *Glia*, *60*(4), 615–629. https://doi.org/10.1002/glia.22295

Kanemaru, K., Kubota, J., Sekiya, H., Hirose, K., Okubo, Y., & Iino, M. (2013). Calcium-dependent N-cadherin up-regulation mediates reactive astrogliosis and neuroprotection after brain injury. *Proceedings of the National Academy of Sciences of the Unites States of America*, *110*(28), 11612–11617. https://doi.org/10.1073/pnas.1300378110

Kanemaru, K., Sekiya, H., Xu, M., Satoh, K., Kitajima, N., Yoshida, K., Okubo, Y., Sasaki, T., Moritoh, S., Hasuwa, H., Mimura, M., Horikawa, K., Matsui, K., Nagai, T., Iino, M., & Tanaka, K. F. (2014). In vivo visualization of subtle, transient, and local activity of astrocytes using an ultrasensitive Ca^{2+} indicator. *Cell Reports*, *8*(1), 311–318. https://doi.org/10.1016/j.celrep.2014.05.056

Kang, J., Jiang, L., Goldman, S. A., & Nedergaard, M. (1998). Astrocyte-mediated potentiation of inhibitory synaptic transmission. *Nature Neuroscience*, *1*(8), 683–692. https://doi.org/10.1038/3684

Klunk, W. E., Bacskai, B. J., Mathis, C. A., Kajdasz, S. T., McLellan, M. E., Frosch, M. P., Debnath, M. L., Holt, D. P., Wang, Y., & Hyman, B. T. (2002). Imaging Abeta plaques in living transgenic mice with multiphoton microscopy and methoxy-X04, a systemically administered Congo red derivative. *Journal of Neuropathology and Experimental Neurology*, *61*(9), 797–805. https://doi.org/10.1093/jnen/61.9.797

Kobayashi, E., Nakano, M., Kubota, K., Himuro, N., Mizoguchi, S., Chikenji, T., Otani, M., Mizue, Y., Nagaishi, K., & Fujimiya, M. (2018). Activated forms of astrocytes with higher GLT-1 expression are associated with cognitive normal subjects with Alzheimer pathology in human brain. *Scientific Reports*, *8*(1), 1712. https://doi.org/10.1038/s41598-018-19442-7

Kuchibhotla, K. V., Lattarulo, C. R., Hyman, B. T., & Bacskai, B. J. (2009). Synchronous hyperactivity and intercellular calcium waves in astrocytes in Alzheimer mice. *Science*, *323*(5918), 1211–1215. https://doi.org/10.1126/science.1169096

Lambert, M. P., Barlow, A. K., Chromy, B. A., Edwards, C., Freed, R., Liosatos, M., Morgan, T. E., Rozovsky, I., Trommer, B., Viola, K. L., Wals, P., Zhang, C., Finch, C. E., Krafft, G. A., & Klein, W. L. (1998). Diffusible, nonfibrillar ligands derived from a 1-42 are potent central nervous system neurotoxins. *Proceedings of the National Academy of Sciences of the United States of America*, *95*(11), 6448–6453. https://doi.org/10.1073/pnas.95.11.6448

Li, S., Hong, S., Shepardson, N. E., Walsh, D. M., Shankar, G. M., & Selkoe, D. (2009). Soluble oligomers of amyloid β protein facilitate hippocampal long-term depression by disrupting neuronal glutamate uptake. *Neuron*, *62*(6), 788–801. https://doi.org/10.1016/j.neuron.2009.05.012

Madroñal, N., Delgado-García, J. M., Fernández-Guizán, A., Chatterjee, J., Köhn, M., Mattucci, C., Jain, A., Tsetsenis, T., Illarionova, A., Grinevich, V., Gross, C. T., & Gruart, A. (2016). Rapid erasure of hippocampal memory following inhibition of dentate gyrus granule cells. *Nature Communications*, *7*, 10923. https://doi.org/10.1038/ncomms10923

Masliah, E., Crews, L., & Hansen, L. (2006). Synaptic remodeling during aging and in Alzheimer's disease. *Journal of Alzheimer's Disease*, *9*(Suppl. 3), 91–99. https://doi.org/10.3233/jad-2006-9s311

Masliah, E., Mallory, M., Hansen, L., Richard, D., Alford, M., & Terry, R. (1994). Synaptic and neuritic alterations during the progression of Alzheimer's disease. *Neuroscience Letters*, *174*(1), 67–72. https://doi.org/10.1016/0304-3940(94)90121-X

Nimmerjahn, A., & Helmchen, F. (2012). In vivo labeling of cortical astrocytes with Sulforhodamine 101 (SR101). *Cold Spring Harbor Protocols*, *2012*(3), 326–334. https://doi.org/10.1101/pdb.prot068155

Nimmerjahn, A., Kirchhoff, F., Kerr, J. N. D., & Helmchen, F. (2004). Sulforhodamine 101 as a specific marker of astroglia in the neocortex in vivo. *Nature Methods*, *1*(1), 31–37. https://doi.org/10.1038/nmeth706

Oberheim, N. A., Takano, T., Han, X., He, W., Lin, J. H. C., Wang, F., Xu, Q., Wyatt, J. D., Pilcher, W., Ojemann, J. G., Ransom, B. R., Goldman, S. A., & Nedergaard, M. (2009). Uniquely hominid features of adult human astrocytes. *Journal of Neuroscience*, *29*(10), 3276–3287. https://doi.org/10.1523/JNEUROSCI.4707-08.2009

Olabarria, M., Noristani, H. N., Verkhratsky, A., & Rodríguez, J. J. (2010). Concomitant astroglial atrophy and astrogliosis in a triple transgenic animal model of Alzheimer's disease. *Glia*, *58*(7), 831–838. https://doi.org/10.1002/glia.20967

Orre, M., Kamphuis, W., Osborn, L. M., Jansen, A. H. P., Kooijman, L., Bossers, K., & Hol, E. M. (2014). Isolation of glia from Alzheimer's mice reveals inflammation and dysfunction. *Neurobiology of Aging*, *35*(12), 2746–2760. https://doi.org/10.1016/j.neurobiolaging.2014.06.004

Osborn, L. M., Kamphuis, W., Wadman, W. J., & Hol, E. M. (2016). Astrogliosis: An integral player in the pathogenesis of Alzheimer's disease. *Progress in Neurobiology*, *144*, 121–141. https://doi.org/10.1016/j.pneurobio.2016.01.001

Pekny, M., Pekna, M., Messing, A., Steinhäuser, C., Lee, J.-M., Parpura, V., Hol, E. M., Sofroniew, M. V., & Verkhratsky, A. (2016). Astrocytes: A central element in neurological diseases. *Acta Neuropathologica*, *131*(3), 323–345. https://doi.org/10.1007/s00401-015-1513-1

Porter, J. T., & McCarthy, K. D. (1996). Hippocampal astrocytes *in situ* respond to glutamate released from synaptic terminals. *Journal of Neuroscience*, *16*(16), 5073–5081. https://doi.org/10.1523/JNEUROSCI.16-16-05073.1996

Prince, G. L., Delaere, P., Fages, C., Duyckaerts, C., Hauw, J.-J., & Tardy, M. (1993). Alterations of glial fibrillary acidic protein mRNA level in the aging brain and in senile dementia of the Alzheimer type. *Neuroscience Letters*, *151*(1), 71–73. https://doi.org/10.1016/0304-3940(93)90048-P

Santello, M., Toni, N., & Volterra, A. (2019). Astrocyte function from information processing to cognition and cognitive impairment. *Nature Neuroscience*, *22*(2), 154–166. https://doi.org/10.1038/s41593-018-0325-8

Schummers, J., Yu, H., & Sur, M. (2008). Tuned responses of astrocytes and their influence on hemodynamic signals in the visual cortex. *Science*, *320*(5883), 1638–1643. https://doi.org/10.1126/science.1156120

Selkoe, D. J., & Hardy, J. (2016). The amyloid hypothesis of Alzheimer's disease at 25 years. *EMBO Molecular Medicine*, *8*(6), 595–608. https://doi.org/10.15252/emmm.201606210

Semyanov, A., Henneberger, C., & Agarwal, A. (2020). Making sense of astrocytic calcium signals—From acquisition to interpretation. *Nature Reviews Neuroscience*, *21*(10), 551–564. https://doi.org/10.1038/s41583-020-0361-8

Shafit-Zagardo, B., Peterson, C., & Goldman, J. E. (1988). Rapid increases in glial fibrillary acidic protein mRNA and protein levels in the copper-deficient, brindled mouse. *Journal of Neurochemistry*, *51*(4), 1258–1266. https://doi.org/10.1111/j.1471-4159.1988.tb03095.x

Shigetomi, E., Patel, S., & Khakh, B. S. (2016). Probing the complexities of astrocyte calcium signaling. *Trends in Cell Biology*, *26*(4), 300–312. https://doi.org/10.1016/j.tcb.2016.01.003

Smit, T., Deshayes, N. A. C., Borchelt, D. R., Kamphuis, W., Middeldorp, J., & Hol, E. M. (2021). Reactive astrocytes as treatment targets in Alzheimer's disease—Systematic review of studies using the APPswePS1dE9 mouse model. *Glia*, *69*, 1852–1881. https://doi.org/10.1002/glia.23981

Stutzmann, G. E. (2006). Enhanced ryanodine receptor recruitment contributes to Ca^{2+} disruptions in young, adult, and aged Alzheimer's disease mice. *Journal of Neuroscience*, *26*(19), 5180–5189. https://doi.org/10.1523/JNEUROSCI.0739-06.2006

Stutzmann, G. E. (2007). The pathogenesis of Alzheimer's disease—Is it a lifelong "Calciumopathy"? *Neuroscientist*, *13*(5), 546–559. https://doi.org/10.1177/1073858407299730

Takano, T., Han, X., Deane, R., Zlokovic, B., & Nedergaard, M. (2007). Two-photon imaging of astrocytic Ca^{2+} signaling and the microvasculature in experimental mice models of Alzheimer's disease. *Annals of the New York Academy of Sciences*, *1097*, 40–50. https://doi.org/10.1196/annals.1379.004

Takano, T., He, W., Han, X., Wang, F., Xu, Q., Wang, X., Oberheim Bush, N. A., Cruz, N., Dienel, G. A., & Nedergaard, M. (2014). Rapid manifestation of reactive astrogliosis in acute hippocampal brain slices. *Glia*, *62*(1), 78–95. https://doi.org/10.1002/glia.22588

Tian, L., Hires, S. A., Mao, T., Huber, D., Chiappe, M. E., Chalasani, S. H., Petreanu, L., Akerboom, J., McKinney, S. A., Schreiter, E. R., Bargmann, C. I., Jayaraman, V., Svoboda, K., & Looger, L. L. (2009). Imaging neural activity in worms, flies and mice with improved GCaMP calcium indicators. *Nature Methods*, *6*(12), 875–881. https://doi.org/10.1038/nmeth.1398

Tyurikova, O., Zheng, K., Rings, A., Drews, A., Klenerman, D., & Rusakov, D. A. (2018). Monitoring Ca(2+) elevations in individual astrocytes upon local release of amyloid beta in acute brain slices. *Brain Research Bulletin*, *136*, 85–90. https://doi.org/10.1016/j.brainresbull.2016.12.007

Verkhratsky, A. (2019). Astroglial calcium signaling in aging and Alzheimer's disease. *Cold Spring Harbor Perspectives in Biology*, *11*(7), a035188. https://doi.org/10.1101/cshperspect.a035188

Verkhratsky, A., & Nedergaard, M. (2018). Physiology of astroglia. *Physiological Reviews*, *98*(1), 239–389. https://doi.org/10.1152/physrev.00042.2016

Wallraff, A., Köhling, R., Heinemann, U., Theis, M., Willecke, K., & Steinhäuser, C. (2006). The impact of astrocytic gap junctional coupling on potassium buffering in the hippocampus. *Journal of Neuroscience*, *26*(20), 5438–5447. https://doi.org/10.1523/JNEUROSCI.0037-06.2006

Wu, Y.-W., Tang, X., Arizono, M., Bannai, H., Shih, P.-Y., Dembitskaya, Y., Kazantsev, V., Tanaka, M., Itohara, S., Mikoshiba, K., & Semyanov, A. (2014). Spatiotemporal calcium dynamics in single astrocytes and its modulation by neuronal activity. *Cell Calcium*, *55*(2), 119–129. https://doi.org/10.1016/j.ceca.2013.12.006

SUPPORTING INFORMATION

Additional supporting information may be found in the online version of the article at the publisher's website.

FIGURE S1 Amyloid-β plaques in the DG can be identified under bright-field conditions. The white arrows in the left panel indicate a structure in the mml of the DG with a more rugged, dense appearance compared to the surrounding tissue. The middle panel shows a methoxy-X04 fluorescence signal at the location of the structure with a rugged, dense appearance, indicating an Aβ plaque. The right panel shows a merge image illustrating the overlap between the rugged, dense structure and the methoxy-X04 signal. Gcl, granule cell layer; mml, middle molecular layer

FIGURE S2 Data indicating the absolute number of astrocytes and astrocyte pairs per slice for all groups (a,b) separately and for 6M and 9M data combined (c,d). Data shown: WT6: ns = 4, $N = 3$; APP6: ns = 9, $N = 3$; WT9: ns = 12, $N = 4$; and APP9: ns = 17, $N = 5$; $^{*}p \leq 0.05$, $^{**}p \leq 0.01$

Transparent Science Questionnaire for Authors

How to cite this article: Huffels, C. F., Osborn, L. M., Cappaert, N. L. & Hol, E. M. (2022). Calcium signaling in individual APP/PS1 mouse dentate gyrus astrocytes increases *ex vivo* with Aβ pathology and age without affecting astrocyte network activity. *Journal of Neuroscience Research*, 100, 1281–1295. https://doi.org/10.1002/jnr.25042